A case study of a Chaco Low Level Jet event

A. Celeste Saulo[1], Marcelo E. Seluchi[2] and Matilde Nicolini[1]

[1]Centro de Investigaciones del Mar y la Atmósfera (CIMA)/ Departamento de Ciencias de la Atmósfera y los Océanos. University of Buenos Aires, Argentina.
[2]Centro de Previsão de Tempo e Estudos Climáticos (CPTEC)/INPE, Cachoeira Paulista. São Paulo, Brazil

Submitted to Monthly Weather Review
Submitted September 2003 - Revised May 2004

Corresponding Author's address
Centro de Investigaciones del Mar y la Atmosfera.
2do piso, pabellon II, Ciudad Universitaria
1428 Ciudad de Buenos Aires
Argentina
E-mail: saulo@at.fcen.uba.ar
Phone: (5411) 4787-2694
Fax: (5411) 4788-3572

Abstract

This paper concentrates on the analysis of the life cycle of the low level jet (LLJ) during a summer Chaco Jet event. This is accomplished through the use of the Eta/CPTEC (Centro de Previsão del Tempo e Estudos Climáticos) regional model, in order to obtain high temporal and spatial detail of the main processes taking place. Both the low level circulation and the geopotential height evolution at different latitudes are analyzed to provide a more detailed description of the effects of topography and differential warming on the evolution of this current.

This study shows that the life cycle of the particular event analyzed, is not the same at the different latitudes swept by this well organized northerly current, expanding from 15ºS to 32ºS during two consecutive days. A common feature to all the examined latitudes is the presence of a diurnal cycle linked to local effects which is more evident during the first day and a half of the simulation. This cycle was identified not only by a nocturnal maximum of the wind, but also by the oscillations of the geostrophic wind close to the surface in response to differential warming over sloping terrain. However, during the second day, the diurnal oscillation is superseded by synoptic scale forcing. The meridional growth of this northerly current reacts basically to a deepening of the Northwestern Argentina Low, consequently being a geostrophic response to a synoptic perturbance. However, during the final stages of this event, a northerly wind area located over the

southern tip of the current, which notably increases the northerlies penetration toward higher latitudes, develops. This last extension is mainly due to a component of ageostrophic origin. Evidence is provided in support to the hypothesis that this secondary development as a feedback between the LLJ and the precipitation at the exit region.

1. Introduction

In recent years there has been a significantly increased interest in the study of the South American low level jet (SALLJ) as a fundamental component of what has come to be named the 'South American Monsoon System'(Nogués-Paegle et al. 2002; Zhou and Lau 1998).

The increased number of studies related to the large scale characteristics of the SALLJ can be partially explained by the availability of analyses and/or reanalyses (i.e., those generated by the National Centers for Environmental Prediction -NCEP- or the European Centre for Medium Range Weather Prediction -ECMWF-). These data sets have also been widely used to describe SALLJ role in the South American climate – particularly in the warm season – and its impact on the hydrological cycle of the La Plata Basin (James and Anderson 1984, Sugahara et al. 1994, Rasmusson and Mo, 1996, Nogués-Paegle and Mo, 1997, Salio et al. 2002, Nicolini et al. 2002, Marengo et al. 2004, Liebmann et al. 2004, among others).

Although there can be found papers based on observational data which mention and/or document the existence of the SALLJ, the fact is that the limited observational network in the region where this current attains its highest intensity, limited previous studies to particular areas close to the synoptic stations (Fernández and Necco 1982; Berri and

Inzunza 1993) or the PACS-SONET special observation network (Douglas et al. 1998; Marengo et al. 2002).

On the other hand, some regional NWP models were able to capture the essential features of the SALLJ and accordingly some of its smaller scale features as well as its diurnal cycle and associated precipitation (Saulo et al. 2000; Berbery and Collini 2000 among others).

So far, the studies performed clearly indicate that the SALLJ is a central component of the tropical-extra tropical exchange in South America, transporting humidity from the Amazon Basin to the La Plata Basin (Seluchi and Marengo, 2000) and increasing precipitation at the exit area of the jet. Previous studies also show that, although the SALLJ is an almost permanent pattern in the summer circulation, its meridional extension is highly variable. Salio et al. 2002 and Nicolini and Saulo (2004, manuscript submitted to J. Geophys. Res.), recognized that the SALLJ penetration toward high latitudes is associated with a deepening of the Northwestern Argentinean Low (NAL) and with a negative geopotential anomaly immersed in mid latitude baroclinic wave trains. The particular SALLJ episodes that exhibit a marked southward penetration have been called Chaco Jet Events (CJE). The CJE criterion requires that the maximum wind intensity be located at some level between surface and 850 hPa. immediately east of the Andes, and be equal or greater than 12 m s^{-1},

originate in low-latitudes and extend to at least 25°S. The criterion also imposes a constraint on the vertical shear: wind speed differences between 850 and 700 hPa and/or between 900 and 700 hPa must be larger than or equal to 6 m s^{-1} in the region encompassed by the 12 m s^{-1} isotach.

Although understanding the mean characteristics of the SALLJ, and particularly those of the CJEs, was relevant – mostly in order to understand their impact on the South Eastern South America (SESA) climate - it is also of interest to progress in the study of the atmospheric boundary layer mechanisms operating during the CJEs and the way in which they are controlled by the synoptic scale patterns. Due to the lack of high resolution observational data in the region, the use of numerical models greatly facilitates this type of analysis. The work by Seluchi et al. 2003 on the analysis of the NAL and its life cycle during two cases of CJEs using the Eta/CPTEC (Eta regional model run at Centro de Previsão del Tempo e Estudos Climáticos) regional model is an example of the proposed approach. In this case, the Eta/CPTEC model proved to be a satisfactory tool for identifying the distinctive signs of these events.

In the summer case-study conducted by Seluchi et al. (2003), it became evident that the thermal low-pressure system is markedly controlled by surface warming thus exhibiting a striking diurnal cycle which is detectable, not only by the evolution of the surface pressure, but also by the associated circulation. However, they also

demonstrated that NAL deepens in response to the approach of an upper level trough at the same time that the low level winds increase their penetration toward higher latitudes. The observed behaviour suggests that the exceptional meridional extension of the CJEs, compared with those of the SALLJ and other low level jets (Stensrud 1996), is a response to a combination of tropical circulation and mid-latitude dynamics, efficiently channelled by the Andes. This is a distinctive characteristic of the South American jets which corroborates their primary role in transporting moisture across the region.

This paper concentrates on the analysis of the life cycle and forcing of the low level jet in the summer Chaco Jet event previously studied by Seluchi et al. 2003. In this way, progress over preceding results is achieved by attempting to evaluate how much of this CJE has a geostrophic origin (i.e., due to the deepening of the NAL or of the Chaco low) and how much is in response to local effects (i.e., diurnal oscillations). The objective is to obtain a more detailed understanding of the timing of this jet in relation to that of the NAL. Likewise it advances toward a more detailed description of the effects of topography and differential warming on the evolution of this current. The paper is organized in the following manner: section 2 briefly describes the model employed; the synoptic evolution, with emphasis on the description of low level circulation and the occurrence of LLJ, is included in section 3; section 4 advances in the detection of local

forcing acting upon the system, whilst section 5 discusses larger scale forcing. Section 6 is a discussion of the results.

2. Brief description of the Eta/CPTEC model and adopted settings

One of the most prominent characteristics of the Eta/CPTEC regional hydrostatic model is the use of the 'eta' vertical coordinate (Mesinger 1984) adopted to reduce the numerical computation problems associated with the pressure gradient force, advection and horizontal diffusion calculation over abrupt slopes.

The model has 38 vertical layers with variable thickness so as to provide better vertical resolution close to the surface and, to a lesser degree, in the proximity of the tropopause. Model topography is represented in the form of steps whose horizontal surfaces coincide with each layer limit. The height of each step is obtained as a mean of the maximum altitudes of the topography within each square of the grid.

Model equations are written on an Arakawa E grid (Arakawa and Lamb, 1977), where the distance between two adjacent mass or momentum points define the grid resolution. In its operative version, which is the one used in this paper, the Eta/CPTEC is integrated with a horizontal grid spacing of 40km.

The temporal integration scheme is split-explicit, where the advective terms and those linked to inertia-gravity waves adjustment are considered separately. Model time step is half of that used for the advective terms (96 seconds in the operative version).

The physics of ETA/CPTEC includes parameterizations for explicit synoptic scale precipitation (Zhao et. al. 1991) and convective scale precipitation according to Betts and Miller (1986) method modified by Janjic (1994). The turbulent exchanges are represented by an updated Mellor and Yamada (1974) scheme (Black 1994), that uses a 2.5 order closure within the boundary layer and in the free atmosphere, and a 2.0 order closure at the levels closest to the ground. The heat and humidity fluxes at the surface are resolved according to Monin-Obukov's method. Short wave and long wave radiation processes are represented by Lacis and Hansen (1974) and Fels and Schwartzkopf (1975) algorithms respectively. For greater details on model parameterizations the reader should consult Staudenmaier (1996).

For the case under study, as in the paper by Seluchi et al. 2003, both the initial and boundary conditions (provided every 6 hours) are taken from the NCEP global analyses. The model was employed in the same domain as its operative version, which is illustrated in Figure 1, and the experiment was started at 0000 UTC February 25, 2000 and ended after 72 hours of simulation. The reader can refer to Seluchi et al. 2003, to see model ability to represent the key aspects of the

system under study. It is considered that model performance is good enough to develop the analysis proposed by this study.

3. Temporal evolution of the low level jet.

Although the synoptic evolution characterizing this event was analyzed in detail by Seluchi et al., 2003, it is interesting to re-evaluate the surface and upper-level circulation aspects which contribute to specifically portray the behaviour, evolution and location of this particular LLJ event.

Figure 2 shows the 850 hPa circulation, with emphasis on the detection of regions satisfying Bonner's (1968) criterion 1, as those where the wind magnitude is greater than 12 m s^{-1} (shaded areas) and the difference in the wind intensity between 850 and 700 hPa (heavy contours) exceeds 6 m s^{-1}.Therefore, the LLJ regions are those in which the shaded areas and the contour lines are superimposed.

Beginning with the first hours of the simulation, there is an organized wind current from the north between 16ºS and beyond 37ºS east of the Andes. Immersed in this current there are two areas that strictly meet the LLJ definition: one of them is located east of the Altiplano (LLJ-ALT) and the other one east of the NAL (LLJ-NAL). A LLJ is first identified at 0600 UTC February 25, 2000 (not shown), east

of the Altiplano. Starting at 1800 UTC of that same day, a jet east of the NAL starts to develop, whilst the LLJ-ALT appears to weaken.

The new system (LLJ-NAL) is visible in Fig. 2a accompanying a deep NAL whose signal is more evident during the warm hours (local time at 64ºW corresponds to UTC-4 hours). In Fig. 2b there can be seen two areas where Bonner criterion 1 is strictly met (i.e. LLJ-ALT and LLJ-NAL), immersed in a well organized and intense northerly wind current which meets the condition to be classified as a CJE. This system weakens in the following hours and by 2100 UTC of the same day, reorganizes and intensifies progressively (Fig. 2c). This occurs concomitantly with a deepening of the NAL, which is accompanied by the LLJ in its propagation toward lower latitudes, consequent to the entrance of cold post-frontal air, starting at 0000 UTC of February 27 (Fig. 2c and Fig. 2d).

In order to complement the description of the low level circulation previously shown, the circulation at 250 hPa is synthesized in Figure 3. A jet-streak can be identified north of the westerly upper level jet, and its location appears to be favourable for a dynamic coupling between the upper level jet and the LLJ-NAL. This kind of coupling effect was initially described by Uccellini and Johnson (1979) who showed that the exit zone of the jet-streak produces a meridional ageostrophic circulation (e.g. with positive sign in the Southern Hemisphere) that could organize a low level jet in the opposite direction (e.g., northerly

in the Southern Hemisphere) by the development of an indirect cell. In the present case, the observed circulation pattern could favour this type of mechanism, particularly at 0600 UTC of February 26 (not shown). It can also be detected both in Fig. 3a as well as in 3b where the maximum LLJ-NAL (Fig. 2a and Fig. 2c) is positioned exactly in the region downstream of the jet streak maximum (though the corresponding exit region is weak in Fig 3b). The presence or absence of this effect will be discussed in subsequent sections.

Analysis of Figures 2 and 3 shows certain independence between LLJ-ALT and LLJ-NAL during the first day of the simulation with a gradual tendency to fusion on the second day (while maintaining individual maxima) concluding as a single current by the end of the period. In both cases there is a change in the spatial scale of the event which is in agreement with its temporal evolution, beginning with locally identifiable LLJ signatures and ending as a synoptic scale feature.

The LLJ-NAL seems to be more closely related to the strength of the NAL and its oscillations throughout the period of study. At the same time, its position with respect to the upper level jet, suggests a dynamic coupling between upper and lower layers. Both the LLJ-ALT and the LLJ-NAL exhibit a diurnal cycle which is clearer during the two first days of the simulation with maxima at different hours, displaying a sustained increase afterwards.

Figure 4 shows the timing of both jets at particular points (indicated by crosses in Fig. 1), and the time evolution of the 850 hPa height and geostrophic v-wind. The choice of these points is motivated by the need to evaluate the LLJ behaviour at different latitudes and to detect its sensitivity to the proximity of the Andes in the west-east direction. Similar cross-sections were performed at various latitudes and longitudes, the selected points being the most significant for this analysis.

On first inspection of the temporal evolution at different locations, northerly winds come out in conjunction with a decreasing tendency of the geopotential height during the first two days. This negative geopotential trend, as expected, is much more noticeable at higher latitudes. A diurnal cycle is superimposed with the height tendency, thus producing an attenuated drop of the geopotential heights during the relatively colder hours. This is clearly observed in all the panels between 0000 UTC and 1500 UTC on February 26, when the geopotential height evolution is distinguished either by an increase (Fig. 4a, b, d, e and f) or by an oscillation that leads to a slight positive tendency (fig. 4c). The meridional wind component is predominantly from the north as is also the geostrophic v-wind, which shows stronger oscillations (occasionally of opposite sign). This behaviour will be further discussed in the following section. In both cases high frequency variations are registered, being more intense at the points close to the topography (Figs. 4a, c and e). These high frequency oscillations are

superimposed with a gradual increase of the northerly wind component during the first day and a half of the simulation.

If the analysis is limited to the strict occurrence of LLJ (see detail in Fig. 4) the latter are fundamentally circumscribed to the points closest to the orography (panels on the left), at least during the first day and a half of the simulation. While theory would predict that the time of the maximum jet should become progressively earlier as one proceeds poleward (Blackadar 1957; Bonner and Paegle 1970), and also states the nocturnal preference for this phenomenon, this can not be conclusively stated in this particular case. The timing of some LLJ episodes immersed in the northerly prevailing flow, can be associated to the referred theory, but some other do not (i.e., the first event in Fig. 4a is detected between 8 and 11 AM local time).

The timing of the LLJ (considering both intensity and shear) does not reflect the timing of the oscillations of the northerly wind intensity alone. In the cases of LLJ-NAL, for example, the intensification of the north wind can be linked to the deepening of the thermal low which, unsurprisingly, becomes more intense at nightfall following the maximum heating hours.

After 1200 UTC February 26, the expected nocturnal preference is not distinguished: an important LLJ is observed around 2100 UTC February 26 at 29ºS (Fig. 4e), which is detected subsequently at almost all points (observed in a SW-NE direction). This LLJ is associated with

the time of minimum geopotential heights for the whole period, particularly at 25º and 29ºS.

Meanwhile, the stations located far from the mountain range, do not show meet the LLJ criteria during the first day and a half, except the event between 0600 and 1200 UTC of February 26 at 63ºW, 29ºS (Fig. 4f), which, in its turn, is strongly controlled by the negative height tendency during this time. It is interesting that during February 27 the stations located toward the east tend to produce an important northerly jet which is very close to satisfying Bonner's criterion in shear, while they exceed it in wind magnitude (see figures 4b, d and f).

The presence of southerlies at 29ºS coincident with LLJ occurrences at 25ºS and 19º, suggests a relationship between these LLJs and the progression of the front, denoting a prefrontal regime with strong northerly winds north of 27ºS and a postfrontal one to the south. The latter becomes evident through an increase in the geopotential height that propagates from the SW to the NE (see Fig. 2d).

4. Analysis of the thermal structure near The Andes slopes

There are a number of papers which refer to the Low-level Jet in the North American Great Plains where different forcing acting on these jets were studied. In principle, and given the fact that there are no

similar studies related to the LLJ east of The Andes (with the exception of the study under ideal conditions presented by Paegle, 1998), it is interesting to analyze which of the mechanisms known for the Northern Hemisphere LLJ, are identifiable here.

Besides the above mentioned role of friction in the diurnal oscillation within the PBL (Blackadar, 1957), other studies demonstrated the existence of a mechanism associated with differential warming over sloping terrains which could influence the intensity of the LLJ (Holton 1967, McNider and Pielke 1981, Zeman 1979). On the other hand, and beyond local effects, different authors (Uccellini and Johnson 1979; Chen et al. 1994; Igau and Nielsen-Gammon 1998, hereafter ING) have distinguished those low level jets characterized by quiescent environments, in which the forcing is clearly local, from those immersed in a synoptically active environment, in which cyclogeneses or frontal systems may develop. In what follows, the forcing mechanisms working in the particular case under study will be analyzed.

To aid in the analysis of these results, it is helpful to synthesize here the central concepts of the paper by McNider and Pielke (1981). These authors show the characteristics of the v-wind and the geostrophic v-wind variations, as a function of height and time of day over a sloping terrain. Following their findings, with prevailing northerly flow over the eastward Andean slope, an increase with height of the geostrophic wind during the warm hours (resulting from the baroclinicity

generated by differential warming) should be expected (e.g., a decrease of the northerly component). This behaviour is not reflected by the real wind due to the effectiveness of mixing during daytime, which causes the winds to be subgeostrophic in this region. On the other hand, at night time, with lesser turbulent mixing, the lower level wind accelerates over and above the surface layer (where the mechanical turbulence is still present). However, with the increased cooling over the sloping terrain, the horizontal pressure gradient in the layers affected by differential cooling reverts, causing a decrease of the geostrophic wind with height (e.g. northerly component increase). The combination of these effects leads to a super-geostrophic wind at night.

Vertical cross sections of potential temperature, v-wind and its geostrophic component at different hours and latitudes are presented to evaluate the incidence of effects related to differential warming. Figure 5 corresponds to 19°S and shows the expected behaviour in the first two panels, with subgeostrophic v-wind closer to the surface within the core during the relatively warmer hours (Figure 5a corresponds to 8 PM local time at 62ºW) and supergeostrophic v-wind in the colder ones (Fig. 5b). During the diurnal hours of the first day, the baroclinicity due to differential warming is evident from the constant potential temperature contours slope of Fig. 5a. Associated with the nocturnal thermal inversion present up to 1200 UTC of February 26, a LLJ develops with

its maximum located just above the inversion (Fig. 5b). The v-wind intensity remains practically unaffected during this period.

However, the evolution during February 26 and 27 differs significantly, since the geostrophic component, although weakened during the cold hour (Fig. 5d) relative to the warm one (Fig. 5c), remains relatively strong and from the north as it is throughout the period of time illustrated by this figure. Meanwhile, the real wind below 800 hPa progressively increases. Toward the morning of February 27 (Fig. 5d), the real wind presents two maxima: one around 900 hPa and another at 800hPa, both following the northerly geostrophic wind pattern, although the 10 m/sec contour in the real v-wind covers a larger area.

The v-wind maximum located around the 750 or 800 hPa could have a geostrophic origin that can be explained by the warm air pool existent over this same area, which is recognized in the 'V' pattern acquired by the constant potential temperature contours (see Fig. 5, nearby the 700 hPa level). This signature is characteristic of an elevated mixing layer (EML) formed by differential warming over the Altiplano (indicated by the curvature of theta contours over the Altiplano in figure 5c, for example) and advected by the westerly flow. This type of EML was described by ING, who located the LLJ at the base of this EML. In any case, this effect would be less important in

this case than in that studied by ING, mainly due to the lower intensity of the westerlies present in this situation (Fig. 5d).

At 25ºS, the northerly v-wind appears to be less related to local and/or surface effects than at lower latitudes, except for denoting a stronger acceleration during nocturnal intervals. Furthermore, the spatial scale of the northerlies core shows a large longitudinal extent that grows continuously during the period under analysis. The axis of the northerly wind maxima is located slightly above the 800 hPa level approaching the surface during the cold hours (i.e., figure 6d) and is supergeostrophic practically at all hours. The geostrophic northerly wind has a marked diurnal cycle very close to the topography. However, from 1200 UTC, February 26 a northerly geostrophic wind region which gradually acquires more intensity and areal coverage is observed. This geostrophic v-wind component moves away from the slopes of the Andes and is not linked to differential warming, though it experiences a more marked diurnal cycle on February 27 than on the previous day. This result would be in agreement with Nicolini and Saulo (2004, manuscript submitted to J. Geophys. Res.) who show that, at these latitudes, the Chaco Jet Events present a stronger diurnal cycle.

At 29ºS (Fig. 7) a LLJ-NAL is observed, with a maximum at relatively warm hours in phase with a maximum of geostrophic wind (Fig. 7a and Fig. 7c) and immersed in a northerly wind current longitudinally extended and deeper in vertical extent (Fig. 7d).

Focusing on warming over the mountain slope and the expected geostrophic response, a very clear signal centred on 65ºW (figures 7a and c) is identified, while an intense northerly geostrophic wind over the higher mountains is evident at 1800 UTC (not shown). During the cold hours (Fig. 7b and Fig. 7d) the northerly wind has a marked ageostrophic character, whereas at 1200 UTC February 27, intense southerlies are observed, consistent with the entrance of the cold air mass.

5. Analysis of non-local effects

The results obtained in the previous section mainly facilitate the recognition of local effects, which are clearer on the first day of the simulation but which do not completely explain the behaviour of the wind on the second day. In order to demonstrate how much of the geostrophic response is associated with a sustained warming or cooling, daily temperature, geopotential height and geostrophic wind changes are shown. The latter were registered between 0000 UTC February 26 and 0000 UTC February 27 and between 1200 UTC February 25 and 1200 February 27. These fields filter the changes associated with the diurnal cycle and highlight the larger scale changes that take place on those days.

The changes at 19ºS shown in Fig. 8a, denote a sustained increase of the northerly geostrophic wind centred on 62ºW below 700 hPa, which is independent of diurnal oscillations. The drop in geopotential height observed leeward of the Andes is largely explained by the presence of an area with increased temperatures located between 700 and 500 hPa. This warmer air mass could have been advected by westerly flow, after being heated over the Altiplano during the warm hours. This effect is even more evident if this analysis is performed between 1800 UTC February 25 and the same hour on February 26 (not shown). Meanwhile, Fig. 8b, shows a stronger negative geopotential tendency also related to warming at middle levels, supporting the hypothesis that, at this latitude, the northerly geostrophic wind does not respond exclusively to the mechanism proposed by McNider and Pielke (1981).

The warming registered at 25ºS during both periods (Fig. 8c and Fig. 8d) is more marked than at 19ºS, as is also the associated drop in geopotential height and the increase of geostrophic wind (in an area co-located with the intense geostrophic winds illustrated in Fig. 6). This warming now has an advective origin since the northerly wind has progressively increased in this latitude during the period of study. This analysis further evidences the geostrophic nature of the LLJ at these latitudes.

Finally, southward, the removal of the diurnal cycle clearly denotes the geopotential drop close to the surface and the significant warming, which covers a vast meridional extension. Again, warming east of 65ºW, is the result of a sustained warm advection which affects the zone during this day (Fig. 8e). This pattern was described by Seluchi et al. (2003) who found an important warm advection effect east of the NAL associated with a persistent northerly geostrophic component which is detected practically throughout the entire period east of 65ºW in the present analysis.

The second period (Fig. 8f) is dominated by the signature of the post-frontal cold air entrance that affects all the variables analyzed. However an area persists east of 62ºW which is still characterized by increased temperatures and an increase in the northerly geostrophic wind centred on 58ºW.

The preceding analysis demonstrates a marked geostrophic component in the periods of highest intensity of the analyzed jet at latitudes north of 25ºS and a strongly ageostrophic character of this current at 29ºS.

The accumulated precipitation field between 1200 UTC February 26 and 1200 UTC February 27 (Fig. 9a) may help us to understand the origin of this intense ageostrophic component. The observed field (Fig. 9b, derived from the rain gauge network from Argentina, Paraguay,

Bolivia, Brazil and Uruguay, available at CPTEC) is included in order to show that, although there are some differences in the location of the observed and the simulated maximum precipitation areas, the intensity is well represented by the model, a fact which demonstrates that the model is a trustworthy tool for the interpretation of physical mechanisms discussed here.

The intense convection that occurred in this period was triggered by the low level convergence noticeable from 2100 UTC February 26 (not shown). The convergence intensifies for several hours as it adopts a NW-SE drift consistent with the frontal orientation verified in Fig. 2d. The observed strong convection may well account for the existence of the ageostrophic acceleration, consistent with the circulation discussed in Figure 7d. To address whether an Uccellini and Johnson (1979) type of coupling could be active or not, the ageostrophic wind was calculated at all levels and the presence of an indirect cell close to the exit region of the upper level jet has been searched. The existence of such and indirect cell would have justified the northerly ageostrophic component of the circulation at low levels around these latitudes, but it could not been detected, in spite of the proximity of the upper level jet streak. It is worth noting that the along-flow wind-speed gradient is rather weak in this jet, and this is a major factor that dictates the strength of the ageostrophic circulation response. This could be an explanation for the absence of this effect in this particular case.

6. Discussion of results

From the previously analyzed features, different forcing mechanisms are recognizable in the development of this Chaco Jet Event. The life cycle of this system is not the same at the different latitudes swept by this well organized northerly current, expanding from 15ºS to 32ºS during two consecutive days, constituting a good example of the tropical-extra tropical exchange which characterizes these CJEs.

A common feature to all points and/or latitudes analyzed is the presence of a diurnal cycle linked to local effects which is more evident during the first day and a half of the simulation. This cycle was identified not only by a nocturnal maximum of the wind, which results from the less effective turbulent mixing at these hours, but also by the oscillations of the geostrophic wind close to the surface in response to differential warming over sloping terrain which are consistent with the theoretical model. However, during the second day, the diurnal oscillation is superseded by synoptic scale forcing, allowing a mesoscale system to achieve the organization and dimensions proper to a synoptic scale.

The meridional extension of this northerly current reacts basically to a deepening of the NAL in agreement with findings of previous studies based on the analysis of the CJE ensembles (Nicolini and

Saulo, (2004, manuscript submitted to J. Geophys. Res.) and Salio et al. (2002). The current study verifies that the associated circulation acquires a geostrophic character. However, as the thermal low moves toward lower latitudes a strong northerly wind persists which is located east of its original position and which presents a marked ageostrophic character that is not explained by a Blackadar type effect. This extension begins to appear between 0300 and 0600 of February 27 in accordance with the first manifestations of the cold air entrance from the southwest. In this way, a strong convergent zone is generated, which is initially detected at 31ºS but gradually affects a wider latitudinal band. Consequently, heavy precipitation is triggered over an area that experienced sustained moist and warm advection from the previous days.

It has been proposed that this precipitation has a positive feedback on the ageostrophic intensification of the wind in the lower levels in accordance with the mechanism invoked by Nicolini et al. (1993). In a numerical case study of the southerly Great Plains low-level jet, these authors analyzed model forecast sensitivity to the presence or absence of latent heating. They found that, although the low level nocturnal jet appears to be established mainly by boundary-layer processes, it is significantly amplified by the condensational latent heat release. Comparison of dry and wet experiments shows that the precipitation effect enhances the low-level cyclonically curved inflow. Recently, Lackmann (2002) analyzed a winter extratropical

cyclone in Central USA and related the low level jet intensification with the latent heat release, using the Ertel potential vorticity (PV) framework. They state that “the location of a PV maximum in the lower troposphere (associated with active convection and consequent large latent heat release), allows associated cyclonic flow east of the PV maximum to contribute to the strength of the LLJ”. This interpretation could also be used in this case, as it is shown by Fig. 10, where a minimum PV center (i.e. maximum cyclonic PV) is clearly located to the east of the LLJ core. This would be the mechanism whereby the Chaco Jet, which can be largely explained geostrophically, shows a portion which notably increases its penetration toward higher latitudes that is mainly due to a component of ageostrophic origin.

Consequently, the Chaco jets are characterized by being deeper than the LLJ locally forced during the night time. The greater depth of the jet in response to the presence of a large scale forcing has been identified in this case study, fundamentally during the last day of the simulation.

In this particular case study, it was found that local forcing dominates the timing of the LLJ during the first day and a half, both at tropical latitudes where it maximizes at dawn (LLJ-ALT) and at middle latitudes (LLJ-NAL) where it maximizes at nightfall. Next, the synoptic scale dynamics control the evolution of this current mainly south of 20ºS. Although it was claimed that the presence of a jet streak at 250

hPa could generate conditions favourable for the organization of the LLJ-NAL and could explain the strongly ageostrophic flow observed at higher latitudes during the last period, no evidence was found for this upper-lower level coupling.

Comparing these findings with documented cases in the Northern Hemisphere, that reveal that LLJs develop in quiescent environments or else occur in synoptically active environments, a combined effect is found in this case: CJEs combine the dynamics of tropical and subtropical zones with those characteristics of middle latitudes. That is, they occur, partly, in quiescent environments (there is an almost permanent LLJ between 15ºS and 20ºS during summer) and partly in active environments (deepening of the thermal low which presents a synoptic scale fluctuation and organized convection at the exit region). Hence the registered temporal and spatial dimensions they achieve in this as in prior studies. The identification of this type of event requires criteria stricter than the substantiation of Bonner's criterion 1 at any one point inasmuch as it combines interactions of various scales.

Although the Eta/CPTEC model adequately represents the essential physical processes of this event, it is also necessary to demonstrate whether the Eta/CPTEC model can indeed capture all the processes which interact in the generation of a CJE. However, it will not be possible to formulate a meaningful answer to this question until high resolution observational data are obtained over this area.

Acknowledgments: This research was partially supported by Program PRUSUL from the Brazilean Science and Technology Ministry, by ANPCYT through Project 07-06671, by the University of Buenos Aires through Projects X055 and X439 and by IAI through Project PROSUR-CRN 055. SALLJEX-Brasil, Projeto de Pesquisa Temático FAPESP (Fundacao de Amparo a Pesquisa do Estado de Sao Paulo) No. 01/13816-1 is also acknowledged for supporting this research. We also appreciate the work done by the reviewers that helped to improve the manuscript.

REFERENCES

Arakawa A. and Lamb V. R., 1977: Computational design of the basic dynamical process of the UCLA general circulation model. *Methods Comput. Phys*., **17**, 173-265.

Berbery, E. H., and E. A. Collini, 2000: Springtime precipitation and water vapor flux over Southeastern South America. *Mon. Wea. Rev*., **128**, 1328-1346.

Berri, G. and J. C. Inzunza B., 1993: The effect of the low-level jet on the poleward water vapour transport in the central region of South America. *Atmos. Env*. Part A, **27A(3)**, 335-341.

Betts A. K. and Miller M. J., 1986: A new convective adjustment

scheme. Part II: Single column test using GATE wave, BOMEX, and arctic air-masses data sets. *Quart. J. Roy. Meteor. Soc*., **112**, 1306-1335.

Black T.L., 1994: NMC Notes: The New NMC mesoscale Eta model: Description and forecast examples. *Wea. Forecasting*, **9**, 256-278.

Blackadar, A. K., 1957: Boundary layer wind maxima and their significance for the growth of nocturnal inversions, *Bull. Amer. Meteor. Soc.*, **38**, 283-290.

Bonner, W. D., 1968: Climatology of the low level jet. *Mon. Wea. Rev*., **96**, 833-850.

Bonner W. and J. Paegle, 1970: Diurnal variations in boundary layer winds over USA in summer. *Mon. Wea. Rev*., **98**, 735 – 744.

Chen, Yi-Leng, Chen, Xin An, Zhang, Yu-Xia, 1994: A Diagnostic Study of the Low-Level Jet during TAMEX IOP 5. *Mon. Wea. Rev*., **122**, 2257-2284.

Douglas, M., W., M. Nicolini, and C. Saulo, 1998: Observational evidences of a low level jet east of the Andes during January-March 1998. *Meteorologica*, **23**, 63-72.

Fernandez A. and G. Necco, 1982: Wind characteristics in the free atmosphere at Argentinean radiosounding stations, (in Spanish). *Meteorologica*, **13**, 7-21.

Fels, S. B., and M. D. Schwarzkopf, 1975: The simplified exchange approximation: A new method for radiative transfer calculations. *J. Atmos. Sci.*, **32**, 1475-1488.

Holton, J. R., 1967: The diurnal boundary layer wind oscillation above sloping terrain. *Tellus*, **19**, 199 – 205.

Igau, Richard C., Nielsen-Gammon, John W., 1998: Low-Level Jet Development during a Numerically Simulated Return Flow Event. *Mon. Wea. Rev.*, **126**, 2972-2990.

James, I. N. and D. L. T. Anderson, 1984: The seasonal mean flow and distribution of large-scale weather systems in the southern hemisphere: the effects of moisture transports, *Quart. J. R. Met. Soc*., **110**, 943-966.

Janjic'. Z. I., 1979: Forward-backward scheme modified to prevent two-grid-interval noise and its application in sigma coordinate models. *Contrib. Atmos. Phys*, **52**, 69-84.

Janjic', Z.I., 1994: The new NMC mesoscale Eta model: Description and forecast examples. *Wea. Forecasting*, **9**, 265-278.

Lacis, A. A., and J. E. Hansen, 1974: A parameterization of the absorption of solar radiation in the earth's atmosphere. *J. Atmos. Sci.*, **31**, 118-133.

Lackmann, G. M., 2002: Cold-frontal potential vorticity maxima, the low-level jet, and moisture transport in extratropical cyclones. Mon. *Wea. Rev*., **130**, 59-74.

Liebmann, B., G. Kiladis, C. Vera, C. Saulo, and L. Carvalho, 2004: Subseasonal Variations of Rainfall in the Vicinity of the South American Low-Level jet and Comparison to the South Atlantic Convergence Zone. *J. Climate*, in press.

Marengo, J., M. W. Douglas, P. L. Silva Dias, 2002: The South American low-level jet east of the Andes during the 1999 LBA-TRMM

and LBA-WET AMC campaign. *J. Geophys. Res.-Atmospheres*, **107**, D20, 47.1- 47.11.

Marengo, J., W. R. Soares, C. Saulo and M. Nicolini, 2004. Climatology of Low-Level Jet east of the Andes as derived from the NCEP reanalyses. *J. Climate*, in press.

McNider, R. T. and R. A. Pielke, 1981: Diurnal Boundary-Layer Development over Sloping Terrain. *J. Atmos. Sci*., **38**, 2198-2212.

Mellor G. L. and T. Yamada, 1974: A hierarchy of turbulence closure model for planetary boundary layers. *J. Atmos. Sci*., **36**, 1722-1735.

Mesinger F., 1984: A blocking technique for representation of mountains in atmospheric models. *Riv. Meteor. Aeronaut*., **44**, 195-202.

Nicolini, M., K. M. Waldron and J. Paegle, 1993: Diurnal oscillations of low-level jets, vertical motion, and precipitation: a model case study. *Mon. Wea. Rev*., **121**, 2588-2610.

Nicolini, M. and A. C. Saulo, 2000. Eta characterization of the 1997-1998 warm season Chaco jet cases. Preprints, *6th International Conf. on Southern Hemisphere Meteorology and Oceanography*, Santiago de Chile, Chile, Amer. Meteor. Soc., 330-331.

_____ , _____, J. C. Torres and P. Salio, 2002: Enhanced precipitation over southeastern South America related to strong low-level jet events characterization during austral warm season. *Meteorologica* - Special Issue on South American Monsoon System, **27**,. 59-70.

Nogués-Paegle, J. and K. C. Mo, 1997: Alternating wet and dry conditions over South America during summer, *Mon. Wea. Rev*., **125**, 2, 279-291.

_____ and Coauthors, 2002. Progress in Panamerican CLIVAR research: Understanding the South American monsoon. *Meteorologica* - Special Issue on South American Monsoon System, **27**, 3-32.

Paegle, J., 1998: A comparative review of South American low level jets. *Meteorologica*, **23**, 73-81.

Rasmusson, E. M., and K. C. Mo, 1996: Large-scale atmospheric moisture cycling as evaluated from NMC global analysis and forecast products, *J. Climate*, **9**, 3276-3297.

Saulo, C., M. Nicolini and Sin Chan Chou, 2000. Model characterization of the South American low-level flow during the 1997-1998 spring-summer season. *Clim. Dyn*., **16**, 867-881.

Salio, P. V., M. Nicolini and C. Saulo, 2002: Chaco low level jet characterization during the austral summer season by ERA reanalysis. *J. Geophys. Res.-Atmospheres*, **107**, D24, 32.1- 32.17.

Seluchi M.E. and J.A. Marengo, 2000: Tropical-Midlatitude Exchange of Air Masses during Summer and Winter in South America: Climatic aspects and examples of intense events. *Int. J. Climatol*, **20**, 1167-1190.

_____, C. Saulo, M. Nicolini and P. Satyamuyty, 2003: The Northwestern Argentinean Low: a study of two typical events. *Mon. Wea. Rev.*, **131**, 2361-2378.

Staudenmaier Jr. M., cited 1996: A Description of the Meso Eta Model, Western Region Technical Attachment, N°96-06, NWSO Sacramento.

[Available on line at http://nimbo.wrh.noaa.gov/wrhq/96Tas/TA9606/ta96-06.html].

Stensrud, D. J., 1996: Importance of low level jets to climate: A review. *J. Climate*, **9**, 1698-1711.

Sugahara, S., R.P. da Rocha and M.L. Rodrigues, 1994: Atmospheric conditions associated with the South America low level jet (in portuguese). *Proc, 7th Congresso Brasileiro de Meteorologia*, Spain, **2**, 573-577.

Uccellini L. and D. Jonhnson, 1979: The coupling of Upper and lower tropospheric jet streaks and implications for the development of severe convective storms. *Mon. Wea. Rev.*, **107**, 682 – 703.

Zeman, O., 1979: Parameterization of the dynamics of stable boundary layers and nocturnal jets. *J. Atmos. Sci.*, **36**, 792-804.

Zhao, Q., and F. H. Carr, 1997: A prognostic cloud scheme for operational NWP Models. *Mon.Wea. Rev.*, **125**, 1931-1953.

Zhou, J., and K.-M. Lau, 1998. Does a monsoon climate exist over South America?. *J. Climate*, **11**, 1020-1040.

Figures Captions:

Figure 1: Model domain and topography (in meters). Points where temporal evolution is analyzed are indicated with crosses. Geographical areas mentioned in the text are included.

Figure 2: 850 hPa geopotential height in mgp. (black contours), and wind barbs (longer barbs correspond to 10 ms^{-1}). Shading corresponds to wind magnitude above 12 m s^{-1}. Wind velocity differences between 850 and 700 hPa above 6 m s^{-1} are thick black dashed. a) 24-hr simulation, verifying at 0000 UTC, 26 February 2000; b) 36-hr simulation, verifying at 1200 UTC, 26 February 2000; c) 48-hr simulation, verifying at 0000 UTC, 27 February 2000 and d) 60-hr simulation, verifying at 1200 UTC, 27 February 2000.

Figure 3: 250 hPa streamlines and wind intensity in m s^{-1} (shaded): a) 24-hr simulation, verifying at 0000 UTC, 26 February 2000 and b) 48-hr simulation, verifying at 0000 UTC, 27 February 2000.

Figure 4: 850 hPa geopotential height (plus sign) , v-wind (open circles) and geostrophic v-vwind (closed circles) temporal evolution at selected points. Thick arrows and black dots in the abscissas indicate periods that satisfy Bonner 1 LLJ criterion.

Figure 5: Vertical cross section at 19°S with topography dark shaded. Wind barbs correspond to horizonal wind at each level (longer barbs correspond to 10 ms^{-1}). Geostrophic v-wind shaded for intensities below -10 m s^{-1} (with white dashed contours) and above 10 m s^{-1} (with white full contours) each 4 m s^{-1} –darker shading corresponding to weaker magnitudes-. Northerly v-wind thick black dashed below -10 m s^{-1} and southerly v-wind thick black contoured above 10 m s^{-1}, each 4 m s^{-1}. Black thin contours show potential temperature (θ) in Kelvin, each 3°. a) 24-hr simulation, verifying at 0000 UTC, 26 February 2000; b) 36-hr simulation, verifying at 1200 UTC, 26 February 2000; c) 48-hr simulation, verifying at 0000 UTC, 27 February 2000 and d) 60-hr simulation, verifying at 1200 UTC, 27 February 2000.

Figure 6: Same as fig. 5 but at 25°S.

Figure 7: Same as fig.5 but at 29°S.

Figure 8: Left panels: vertical cross section of geostrophic v-wind change (shaded with white dashed for northerlies below -2 m s^{-1}, each 4 m s^{-1}) temperature change (thick black contours) and geopotential height change (thin black contours) between 0000 UTC, 26 February 2000 and 0000 UTC 27 February 2000. Right panels: same as right ones but for changes between 1200 UTC, 26 February 2000 and 1200 UTC 27 February 2000. a) and b): cross section at 19°S, c) and d) cross section at 25°S and e) and f) cross section at 29°S.

Figure 9: 24 hr-Accumulated precipitation (in mm) from 1200 UTC 26 February 2000 to 1200 UTC 27 February 2000. a) observed; b) simulated with Eta/CPTEC model.

Figure 10: Vertical cross section at 29°S with topography dark shaded corresponding to the 60-hr simulation, verifying at 1200 UTC, 27 February 2000. Ertel potential vorticity shaded for values below -2 PVU (Potential Vorticity Units = 1.0 x 10^{-6} m^2 s^{-1} K kg^{-1}) each 2 PVU –darker shading corresponding to weaker magnitudes-. Northerly v-wind thick black dashed below -10 m s^{-1}. Black thin contours show potential temperature in Kelvin, each 3°.

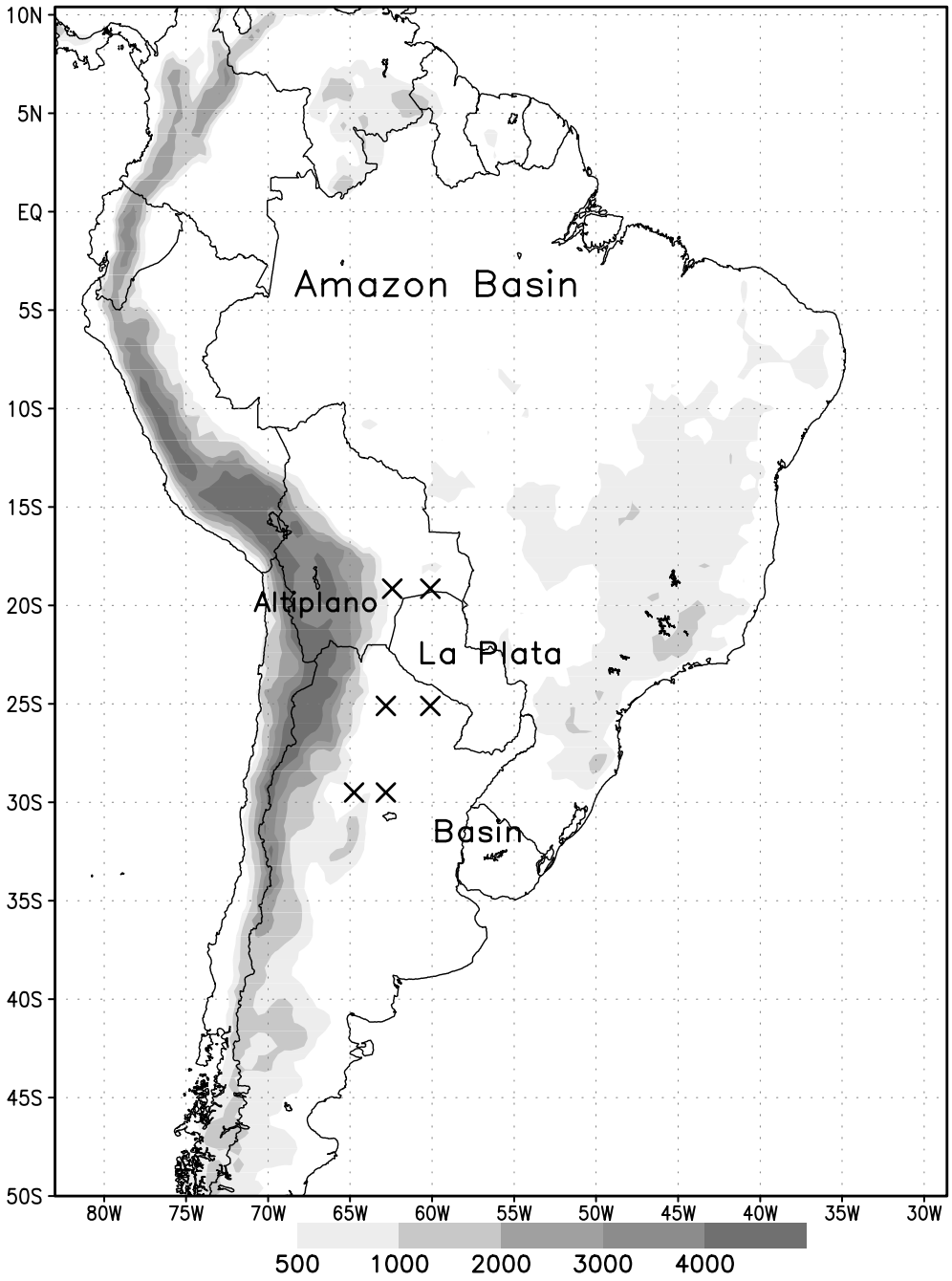

Figure 1: Model domain and topography (in meters). Points where temporal evolution is analyzed are indicated with crosses. Geographical areas mentioned in the text are included.

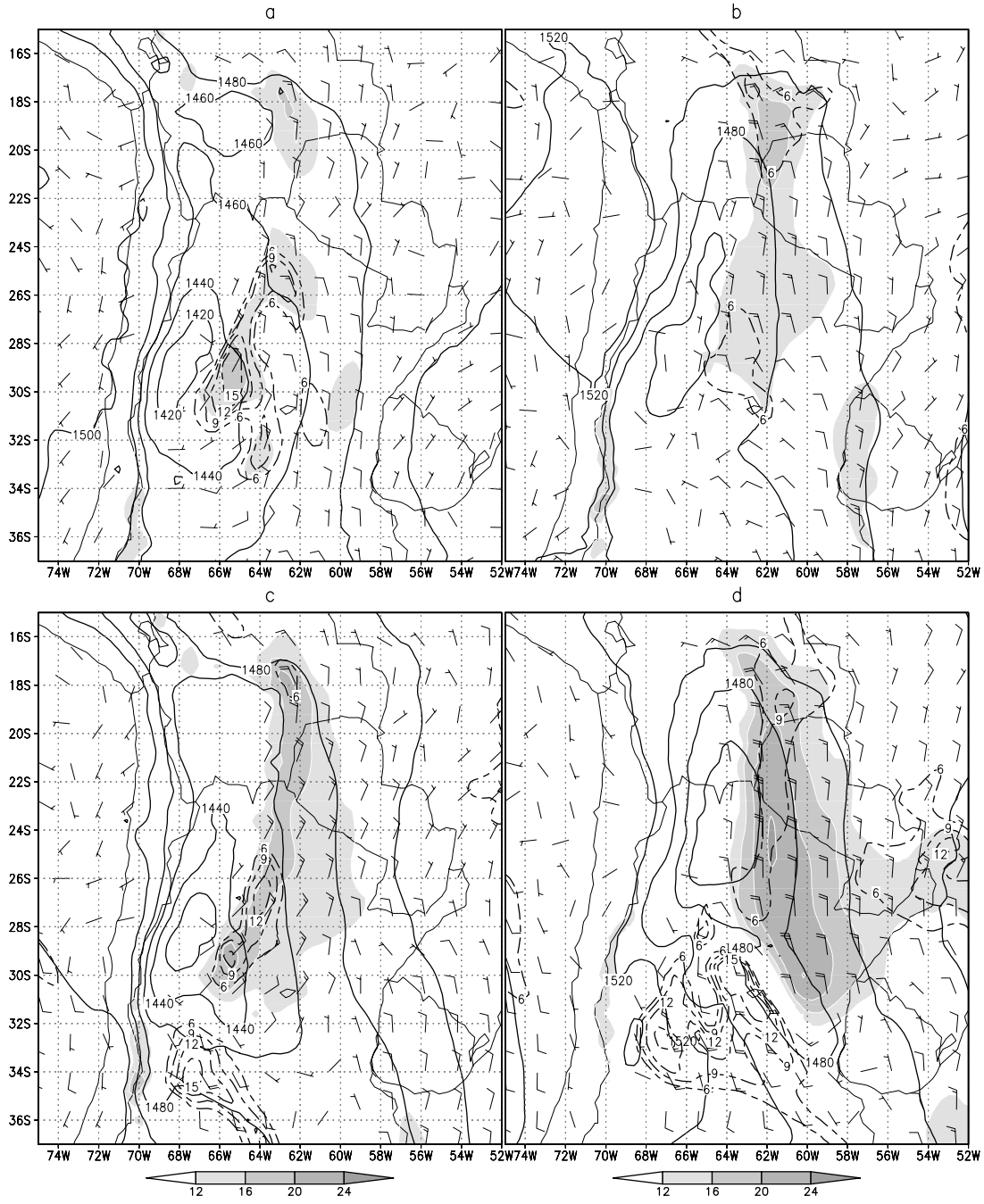

Figure 2: 850 hPa geopotential height in mgp. (black contours), and wind barbs (longer barbs correspond to 10 ms^{-1}). Shading corresponds to wind magnitude above 12 m s^{-1}. Wind velocity differences between 850 and 700 hPa above 6 m s^{-1} are thick black dashed. a) 24-hr simulation, verifying at 0000 UTC, 26 February 2000; b) 36-hr simulation, verifying at 1200 UTC, 26 February 2000; c) 48-hr simulation, verifying at 0000 UTC, 27 February 2000 and d) 60-hr simulation, verifying at 1200 UTC, 27 February 2000.

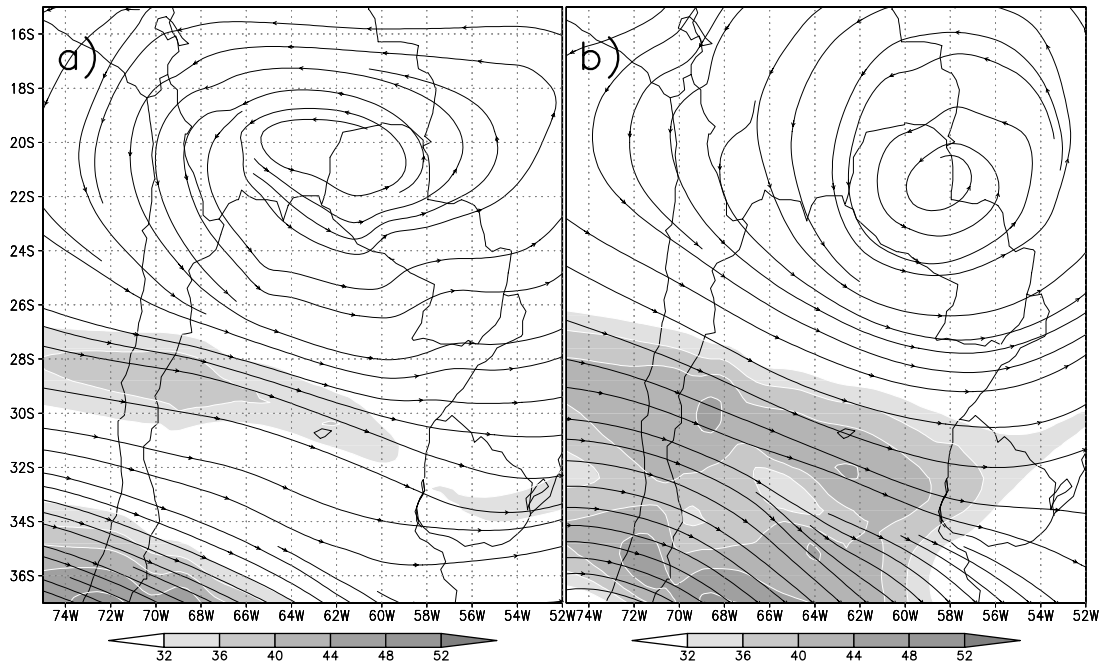

Figure 3: 250 hPa streamlines and wind intensity in m s^{-1} (shaded): a) 24-hr simulation, verifying at 0000 UTC, 26 February 2000 and b) 48-hr simulation, verifying at 0000 UTC, 27 February 2000.

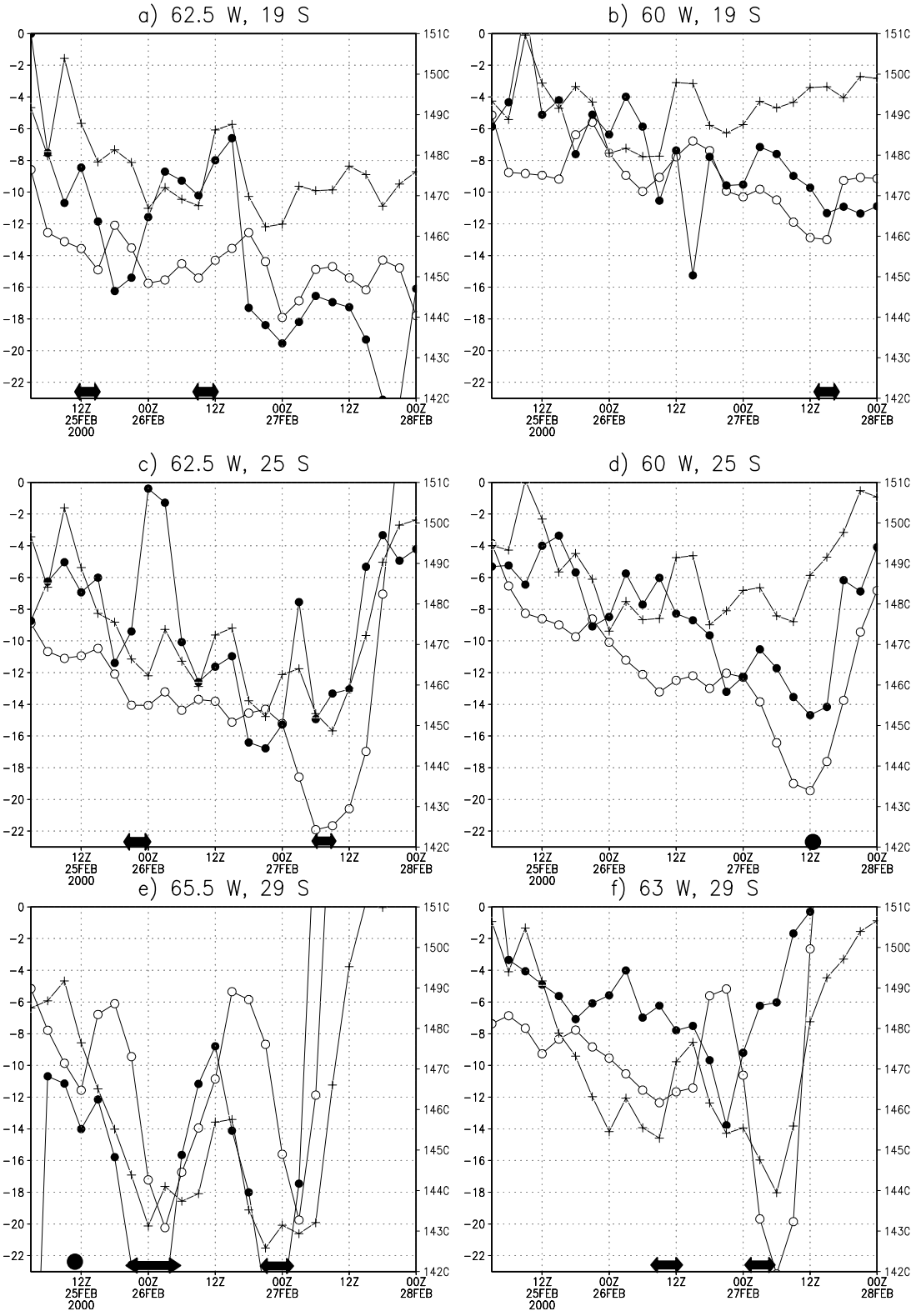

Figure 4: 850 hPa geopotential height (plus sign) , v-wind (open circles) and geostrophic v-vwind (closed circles) temporal evolution at selected points. Thick arrows and black dots in the abscissas indicate periods that satisfy Bonner 1 LLJ criterion.

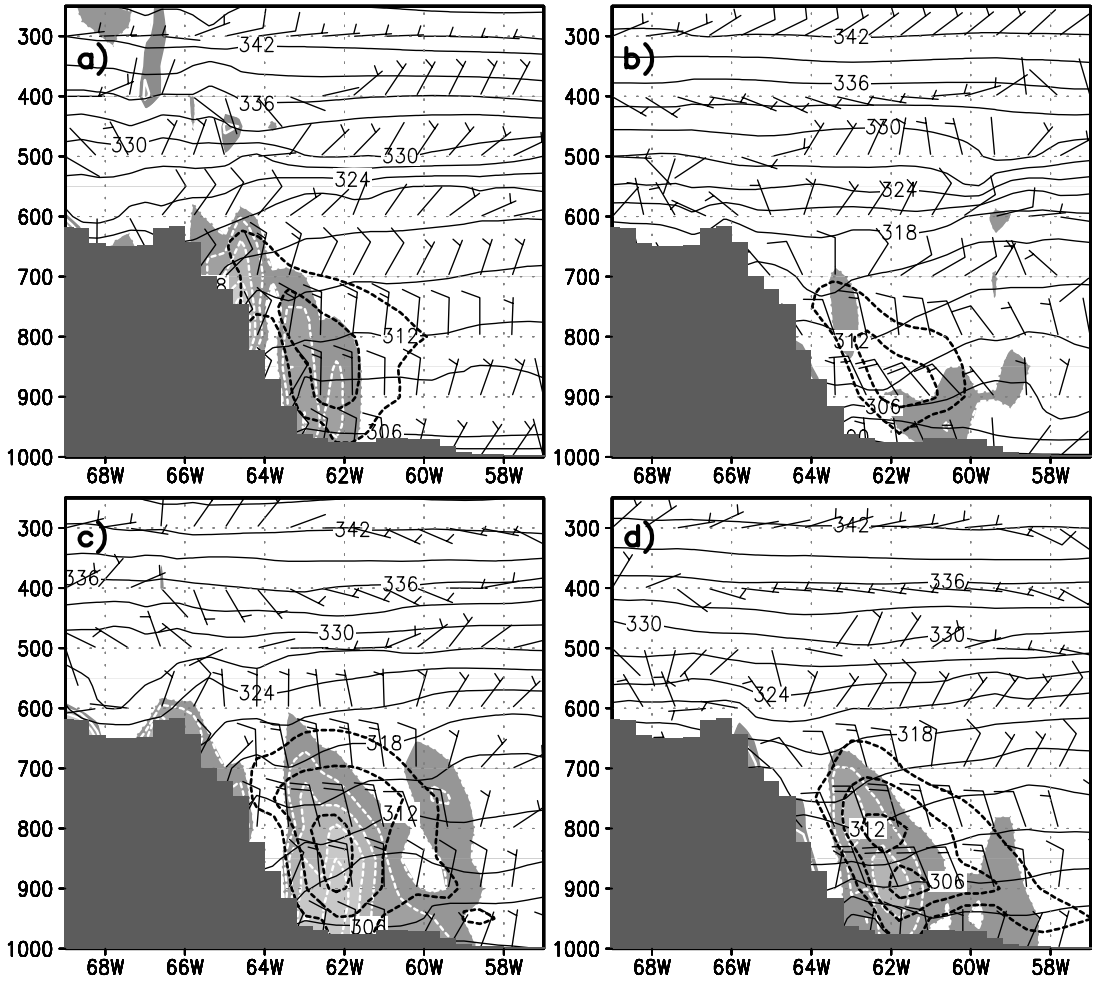

Figure 5: Vertical cross section at 19°S with topography dark shaded. Wind barbs correspond to horizonal wind at each level (longer barbs correspond to 10 ms^{-1}). Geostrophic v-wind shaded for intensities below -10 m s^{-1} (with white dashed contours) and above 10 m s^{-1} (with white full contours) each 4 m s^{-1} –darker shading corresponding to weaker magnitudes-. Northerly v-wind thick black dashed below -10 m s^{-1} and southerly v-wind thick black contoured above 10 m s^{-1}, each 4 m s^{-1}. Black thin contours show potential temperature (θ) in Kelvin, each 3°. a) 24-hr simulation, verifying at 0000 UTC, 26 February 2000; b) 36-hr simulation, verifying at 1200 UTC, 26 February 2000; c) 48-hr simulation, verifying at 0000 UTC, 27 February 2000 and d) 60-hr simulation, verifying at 1200 UTC, 27 February 2000.

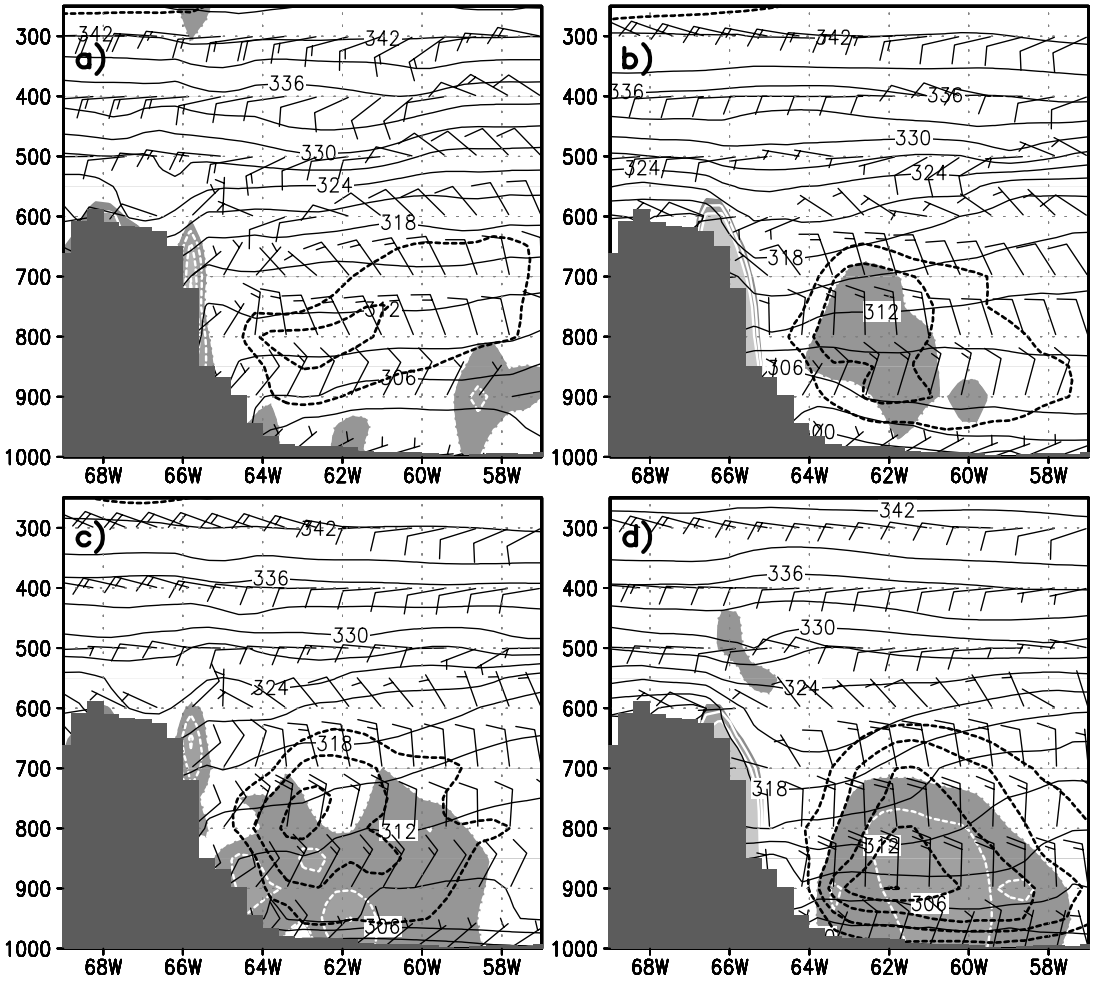

Figure 6: Same as fig. 5 but at 25°S.

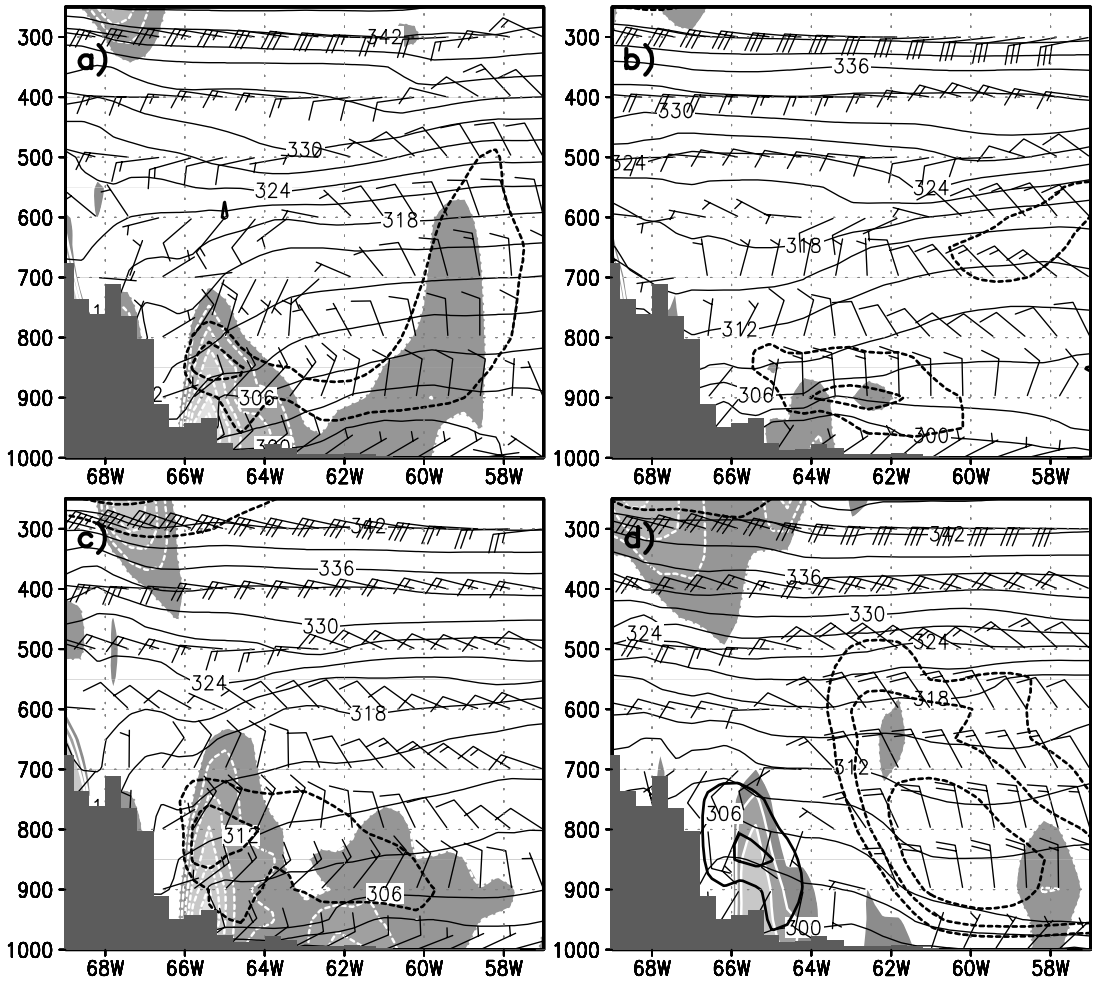

Figure 7: Same as fig.5 but at 29°S.

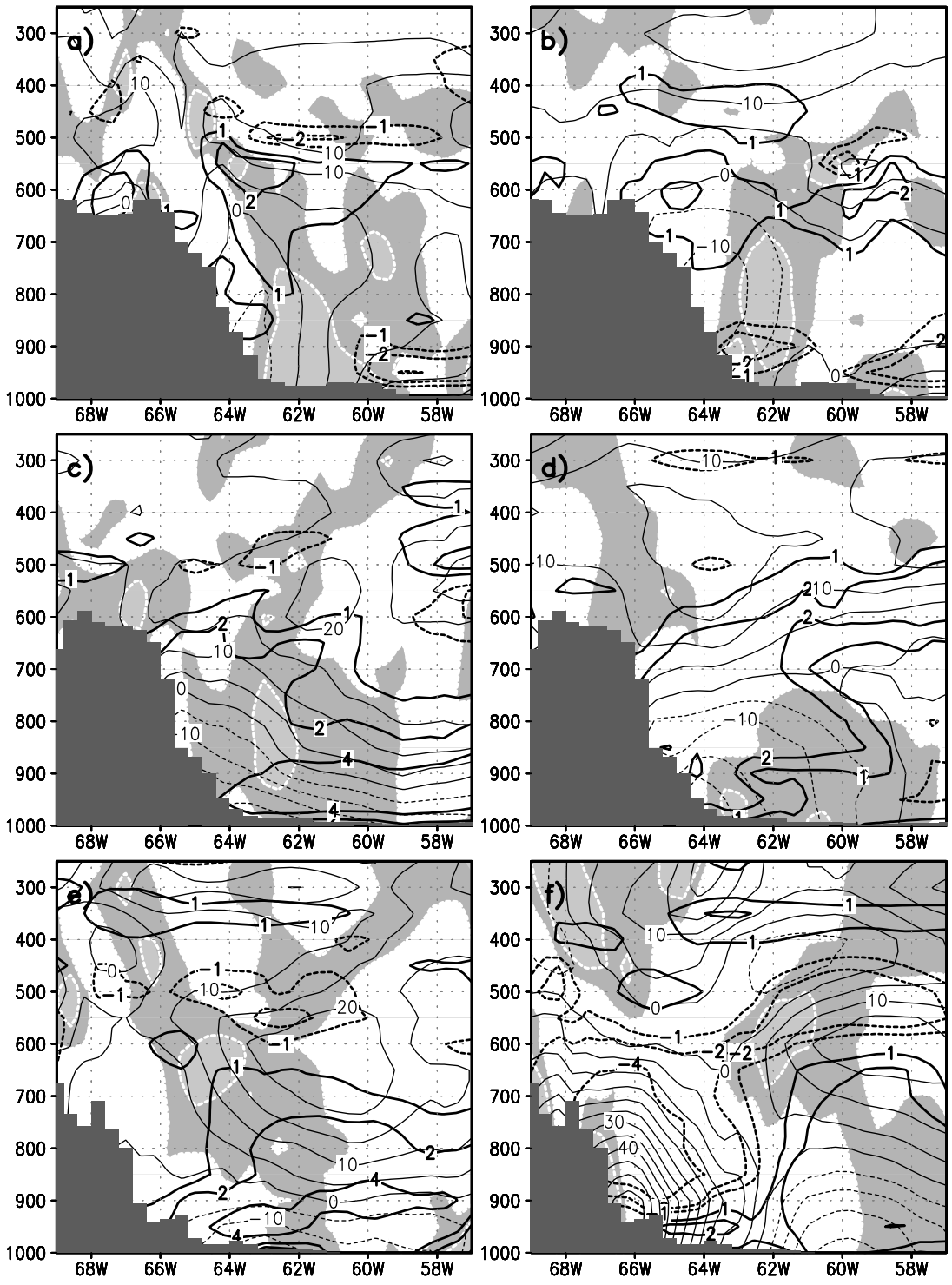

Figure 8: Left panels: vertical cross section of geostrophic v-wind change (shaded with white dashed for northerlies below -2 m s^{-1}, each 4 m s^{-1}) temperature change (thick black contours) and geopotential height change (thin black contours) between 0000 UTC, 26 February 2000 and 0000 UTC 27 February 2000. Right panels: same as right ones but for changes between 1200 UTC, 26 February 2000 and 1200 UTC 27 February 2000. a) and b): cross section at 19°S, c) and d) cross section at 25°S and e) and f) cross section at 29°S.

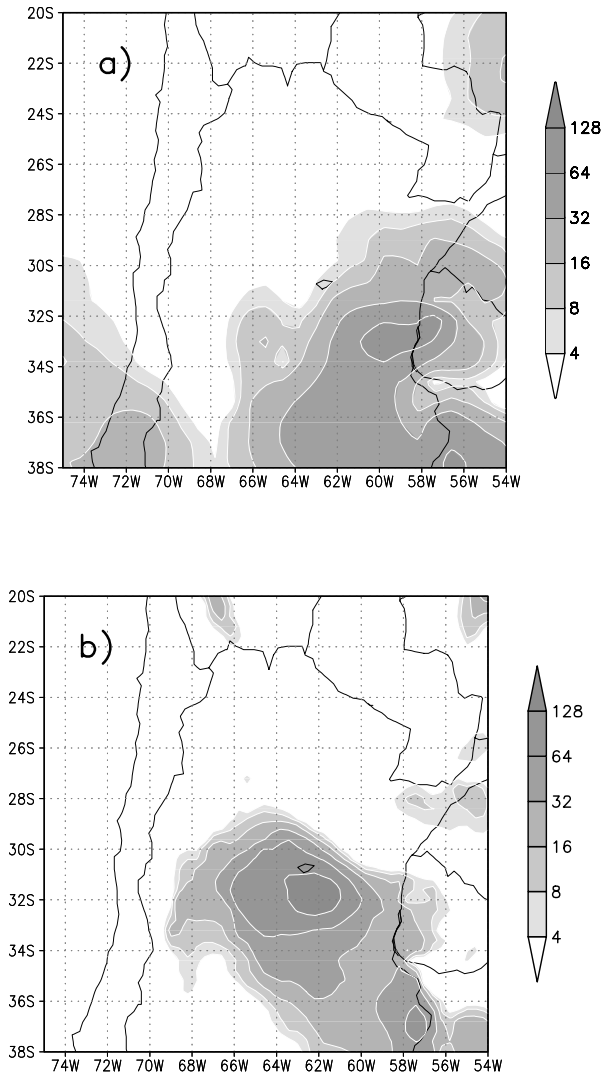

Figure 9: 24 hr-Accumulated precipitation (in mm) from 1200 UTC 26 February 2000 to 1200 UTC 27 February 2000. a) observed; b) simulated with Eta/CPTEC model.

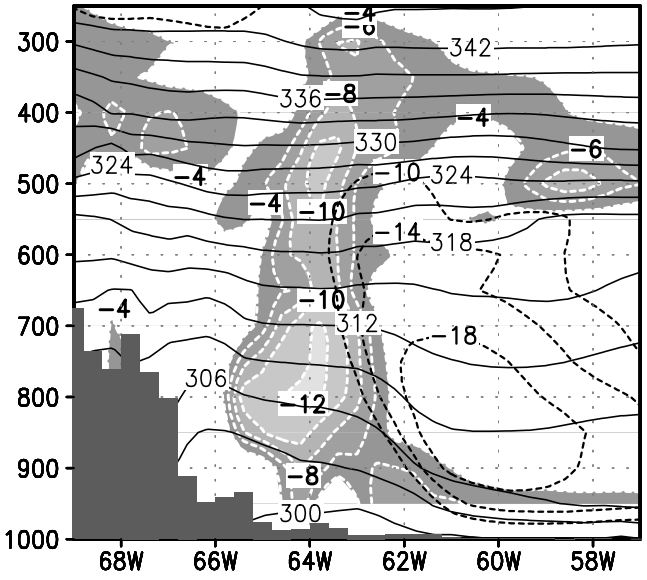

Figure 10: Vertical cross section at 29°S with topography dark shaded corresponding to the 60-hr simulation, verifying at 1200 UTC, 27 February 2000. Ertel potential vorticity shaded for values below -2 PVU (Potential Vorticity Units = 1.0 x 10^{-6} m^2 s^{-1} K kg^{-1}) each 2 PVU –darker shading corresponding to weaker magnitudes-. Northerly v-wind thick black dashed below -10 m s^{-1}. Black thin contours show potential temperature in Kelvin, each 3°.